N93-13686

PLANAR LASER-INDUCED FLUORESCENCE IMAGING OF OH IN THE EXHAUST OF A BI-PROPELLANT THRUSTER

P. H. Paul and N. T. Clemens
Combustion Research Facility
Sandia National Laboratories
Livermore, CA 94550

D. B. Makel
Aerojet Propulsion Division
Gencorp Aerojet
Sacramento, CA 95813

SUMMARY

Planar laser-induced fluorescence imaging of the hydroxyl radical has been performed on the flow produced by the exhaust of a subscale H_2/O_2 fueled bi-propellant rocket engine. Measurements were made to test the feasibility of OH (0,0) and (3,0) excitation strategies by using injection seeded XeCl and KrF excimer lasers, respectively. The flow is produced with hydrogen and oxygen reacting at a combustor chamber pressure of 5 atm which then exhausts to the ambient. The hydroxyl concentration in the exhaust flow is approximately 8%. Fluorescence images obtained by pumping the $Q_1(3)$ transition in the (0,0) band exhibited very high signals but also showed the effect of laser beam absorption. To obtain images when pumping the $P_1(8)$ transition in the (3,0) band it was necessary to use exceptionally fast imaging optics and unacceptably high intensifier gains. The result was single-shot images which displayed a signal-to-noise ratio of order unity or less when measured on a per pixel basis.

INTRODUCTION

Measurement techniques based on planar laser-induced fluorescence (PLIF) imaging provide a powerful tool for the study of complex reacting gaseous flows. In addition to the wide use of PLIF for flow visualization, there is also a growing body of work which has concentrated on developing PLIF spectroscopic strategies to measure species concentration, temperature, pressure and velocity[1]. The present effort is directed towards the evaluation of these techniques for application to flows produced by hydrogen-fueled rocket engines. Poor injector mixing, flow stratification, and excess fuel film cooling in these engines represent a performance loss which reduces the engine specific impulse. High oxidizer concentrations near the thrust chamber wall and in the nozzle, which result from poor mixing or injector maldistribution, can result in reduced engine life.

Cold flow imaging studies have been performed using particulates* or molecular tracers (e.g. iodine or NO). However, for actual engine evaluation, a nascent molecular species is required. Of particular interest is the hydroxyl radical; the concentration distribution of OH may be viewed as a zero'th order indicator of mixture fraction in the high temperature gases. Further, OH is an excellent candidate for PLIF temperature and velocity imaging[2]. In the following we describe the results of OH imaging experiments using (0,0) and (3,0) excitation performed with injection seeded XeCL and KrF excimer lasers, respectively. The measurements were made in the exit plane of a subscale O_2/H_2 engine. The high temperature, supersonic flow studied here is similar to the conditions encountered in large scale engines.

For an optically thin medium, the fluorescence signal on a per laser pulse basis may be written as,

$$S_f = C_{opt} f_B(T) E_p B g_{al} \chi_a n_0 g_D A/(A+Q+V+P) (1 - H(E_pB)) \quad (1)$$

Here C_{opt} is a collection of constants which describe the optical system, f_B is the Boltzman fraction in the ground ro-vib state, E_p is the laser energy, B is the Einstein coefficient for absorption, $\chi_a n_0$ is the number density of the absorbing species, g_D is the detector spectral response fraction, and P is the excited state predissociation rate. The other terms in equation 1 must be thought of as functions of field variables $\underline{F}$; that is they depend on the local distribution of temperature, pressure and perturbing species mixture fraction. Thus $g_{al}(\underline{F})$ is the convolution of the absorption and laser spectral profiles which also depends on velocity through the molecular Doppler-shift, $A(\underline{F})$ is the effective spontaneous emission rate, $Q(\underline{F})$ is the collisional quenching rate, $V(\underline{F})$ is the excited state vibrational transfer rate and $H(E_pB,\underline{F},\tau_{las})$ is a correction which goes to zero in the limit of weak pumping.

By using various pump/detection strategies, different terms in equation 1 can be made dominant. Here the cases of particular interest are termed 'predissociation' and 'quenching' dominated. These are to first order

$$\begin{aligned} S_f &\propto f_B(T) \chi_a n_0 \quad ; \quad P >> A+Q+V \\ S_f &\propto f_B(T) T^{-\alpha} \chi_a \quad ; \quad P = 0, \;\; Q+V >> A \end{aligned} \quad (2)$$

In both cases, careful selection of the ro-vib transition can be used to minimize the stray temperature dependence giving images that primarily represent OH number density or mixture fraction, respectively. The predissociation limit is attractive since the infuence of collisional effects can be removed[3]. For flow visualization studies, these are adequate descriptions of how the signal depends on field variables. Even when the image has a secondary dependence on temperature or mixture fraction such data can still be used effectively to study flowfield topology[4]. To extend the technique to a 'quantitative' measurement requires a much more detailed approach to both the

* D. B. Makel and I. M. Kennedy, 'Cold flow mixing measurements for a swirl triplet liquid rocket gas generator system,' (submitted to AIAA Journal of Propulsion and Power, 1992).

fluorescence model and to imaging system performance[5]. We will address some of these issues in the discussion below.

EXPERIMENTAL APPARATUS

Sets of images using single laser shot PLIF of OH were obtained using two different excitation strategies. The first scheme uses the injection seeded XeCl excimer (Lambda Physik, EMG 150 T MSc) to excite the $Q_1(3)$ transition in the OH $A^2\Sigma \leftarrow X^2\Pi$ (0,0) band. Broadband detection was employed and the images were recorded with an f/4.5 lens (Nikon, UV-Nikor) on a custom-built gated intensified CCD array operating in an RS-170 format. Images were digitized to 8-bits with a Data Translation DT2851 frame grabber in an PC/AT computer. This technique has been used before for reacting flow studies[4] and for PLIF velocity imaging[2]. The second scheme uses the same laser operated on KrF to excite the $P_1(8)$ transition in the OH $A^2\Sigma \leftarrow X^2\Pi$ (3,0) band. These measurements were made with the same camera now equipped with a long pass filter (1 mm Schott WG-280) which was required to reject Rayleigh scattering and a custom built f/1.2 imaging lens. PLIF measurements of OH using this later method have been reported by Andresen et al.[6] and single point LIF measurements have been reported by Pitz et al.[7]

The experimental setup is shown in figure 1. The laser and camera were operated in a 60 Hz mode. The laser beam was expanded into a 10 cm high sheet which was positioned to bisect the engine exhaust plume. The sheet thickness was estimated to be 0.4 mm full-width at $1/e^2$. Line tuning was optimized using a propane torch during pretest and checked post-test. A schematic of the subscale engine (5 lbf motor with an expansion ratio of 1.8:1) is shown in figure 2. The engine consists of an integral spark ignitor/injector, a water cooled combustion section, and a water-cooled nozzle. The oxidizer is injected on the centerline through the gap formed by the ignitor electrode and the engine body. The fuel is injected radially into the oxidizer flow and downstream of the spark gap. The combustion chamber is designed with a turbulence ring to promote mixing. The nozzle used for the present study has a 5 mm throat made of a ZrCu alloy and the external nozzle body is tapered to minimize interference to the laser sheet and imaging optics. The combustion chamber can be operated at pressures up to 10 atm producing flow Mach numbers in excess of 2 in the exit plane.

The flow conditions used for the present study were: $P_0 = 72$ psia, $f(O_2) = 182$ SLPM, $f(H_2) = 182$ SLPM. These give a mixture ratio of 8.0 and exit plane conditions calculated to be: $T_{static} = 2670$ K, $P_{static} = 8$ psia, $v = 2560$ m/s and $M = 1.95$. Species mole fractions in the exit plane were calculated from equilibrium to be: 0.08, 0.70, 0.03, 0.11, 0.04, and 0.02 for OH, H_2O, O_2, H_2, H and O, respectively. During the runs the oxygen flowrate was metered using a mass flow controller and the hydrogen flowrate was controlled with a sonic orifice. Engine temperatures and pressures were digitized and stored on a computer. Chamber ignition was performed with an oxygen lead to minimize the exhaust of unreacted hydrogen. Nitrogen flows controlled by check valves were used to automatically purge the engine at start-up and shut-down.

EXPERIMENTAL RESULTS

Figure 3 is a conventional time-exposure photograph of the exhaust plume which shows the diamond shock structure characteristic of an over-expanded jet. The luminosity of the plume is apparent to the eye for over 25 cm downstream of the nozzle, although the last visible shock diamond is seen at approximately 7.5 cm downstream. Figure 4 shows two representative single-shot PLIF images obtained by using (0,0) excitation. The signal levels are very high and required the use of a low intensifier gain to prevent saturation of the CCD camera. The high signal level becomes apparent when one considers that resonant detection is being used thus: the bright spots which turn to black at their center are the result of scattering from water droplets which are regularly ejected by the engine; while the faint blur seen at the bottom of the images is the nozzle body which scatters some stray laser light (the laser sheet being cut-off at approximately 0.5 cm above the engine). One may also notice a systematic left-to-right attenuation in the signal, the result of a large absorption coefficient for the $Q_1(3)$ line (of order 100 cm^{-1} atm^{-1}). These images are quite similar to that which would be obtained in a simple zero-heat-release reactive mixing experiment. Downstream of the potential core, intrusions of ambient air are seen to cut completely across the jet which often exhibit behavior similar to 'flame-tip' burnout or separation. No evidence of the diamond shock pattern is seen in these images since the primary signal dependence is on OH mole fraction and temperature, the latter being only slightly modulated in the weak shocks present in this flow.

Figure 5 shows two representative single-shot PLIF images obtained by using (3,0) excitation. The difference from the previous data set is dramatic. The recorded signal levels are exceptionally low and as a result are subject to strong signal shot noise. This is apparent when one considers that these images were obtained using a microchannel plate (MCP) gain in excess of 1500 e^-/e^-, thus the pattern in the background is likely the result of thermal emission from the MCP. Further it is possible to again see evidence of the engine nozzle, this being the result of secondary scattering of the OH emission or scattered laser light as collected through a filter attenuation of order 10^{-5}. A 15-frame average of images taken with (3,0) excitation, given in figure 6, shows some evidence of the diamond shock structures as the signal is now directly dependent on total density. However the noise level in this averaged image is still of order 20% peak-to-peak of the total signal variation seen across the first diamond shock (see figure 7). It is also of note that when the long-pass filter was removed the Rayleigh scattering from the ambient room air overwhelmed the OH PLIF signal, and it was possible to readily observe the drop in Rayleigh signal in the low density engine exhaust gases.

DISCUSSION

For the (0,0) pumping case, an f/4.5 lens was used and the intensifier MCP gain was approximately 50 e-/e-. While for the (3,0) pumping case an f/1.2 lens was used and the intensifier gain was approximately 1500 e-/e-. The fraction of the $v'=3$ emission collected through the

longpass filter was estimated by a weighted sum of the product of filter spectral transmission and band lifetimes and found to be 78%. We find the ratio of the measured signals on an equal imaging system basis to be $S_{f(0,0)}/S_{f(3,0)} \approx 350$. Using the predictions given by Seitzman[8] and adjusting the (0,0) quenching rate to reflect the conditions studied here ($Q(H_2O) \approx 1.68$/ns and $Q(H) \approx 0.19$/ns; see Appendix A) we find a value of $S_{f(0,0)}/S_{f(3,0)} \approx 524$ which is in reasonable agreement with the experimental observation. We expect the measured value to be somewhat lower than the prediction since some degree of depopulation of the ground-state with (0,0) pumping should occur in the experiment.

The quality, that is the spatial resolution and signal-to-noise performance, of the images obtained in these experiments has a direct impact on the ability to use such data for quantitative measurements. In both of the cases described above the image data is in the signal-shot-noise limit. Thus the signal-to-noise ratio on a per-pixel basis is given by $S/N = \sqrt{(\eta\ S_f / \kappa(G))}$, where η is the detector quantum efficiency and κ is the intensifier noise factor[5]. The useful signal dynamic range, D_s, is defined to be the ratio of that signal which produces a non-recoverable saturation to that signal which gives an S/N of unity, $D_s \approx C_s\ S(G) / (G\ \kappa(G))$[5]. Here C_s is a constant which depends on the details of the camera system, S is an MCP saturation function and G is the MCP electron gain. Values for the conditions used in the present experiment were evaluated using a model for the image and signal transfer function of intensified cameras[5]. For the (0,0) pumping experiment we find $\kappa \approx 3.7$ and $D_s \approx 114$. In this case the S/N could have actually been improved by a slight increase in lens f-number with a commensurate increase in MCP gain. For the case of (3,0) pumping we find $\kappa \approx 2.2$ and $D_s \approx 4$. For this later case the severe compression in dynamic range would preclude a quantitative measurement even if the S/N were improved. The modulation transfer function, which quantifies the ability of the imaging system to transfer object contrast to the image, for the fast lens used for the (3,0) experiment is calculated to be significantly worse than that obtained in the (0,0) experiment. This observation is with regard to both the blur spot radius and to the shape of the function at intermediate spatial frequencies. Even if the S/N were improved in the (3,0) experiment, significant systematic errors would occur in taking gradients to obtain scalar dissipation or using ratiometric image processing to obtain temperature as a direct result of the contrast reduction.

In the present experiment, the OH is found in a bath composed mostly of water vapor, however the effect of collisions with the radicals cannot be disregarded. For the conditions at the nozzle exit the predominant electronic quencher is water followed by atomic hydrogen and the conventional view would be that vibrational energy transfer (VET) could be neglected. However, OH is present at 8% and both OH-A and OH-X states have large dipole moments; thus a noticeable VET rate is expected as a result of 'near-resonant' electronic energy transfer (e.g. $OH^{*\dagger} + OH \rightarrow OH^{\dagger} + OH^{*}$ where the asterisk denotes electronic excitation and the dagger denotes vibrational excitation)[9]. This process can be quite effective and has been observed in NO[10]. Using the model of Cross and Gordon[11] we estimate a contribution to the total VET rate of

$V_3 = V_{32} + V_{31} + V_{30} \approx 0.12$/ns due to collisions with OH $X^2\Pi$ at the engine nozzle exit conditions. Upon mixing with the ambient air the temperature and radical population in the exhaust products will drop and N_2 and O_2 will be introduced as collision partners. For $v'=3$ and conditions found in H_2/air post flame products at atmospheric pressure, we estimate that the total VET rate due to N_2 to be near equal to the electronic quenching rate due to H_2O. Evidence for effective VET from $v'=3$ can be seen in OH fluorescence dispersion spectra obtained in laminar H_2/O_2 and butane/air flames†. For the butane flame, emission in the (0,0) band is larger than emission in the (1,1) band which is noticeably larger than emission from $R_2(6)$ (3,3). This result is likely due to the presence of CO_2 and suggests that multiple VET steps are occurring. In the H_2/O_2 flame, emission in the (0,0) and (1,1) bands is near equal and both are smaller than emission from $R_2(6)$ (3,3). The later result is consistent with the measurement having been made in a laminar flame with near equilibrium OH concentrations and without the presence of N_2.

For the range of 1400 K to 2700 K we do not expect a strong variation in the $v'=0$ quenching rate for the ambient air or the engine exhaust products except as occurs due to the loss of the atomic hydrogen as a collision partner. We estimate that the effective quenching cross-section will decrease by no more than 10% from conditions at the nozzle exit plane to conditions of an equal mixture of frozen exhaust products with room air. Thus the variation in signal using (0,0) pumping depends directly on OH mole fraction and on $f_B(T)/\sqrt{T}$. This latter function goes approximately as $T^{-1.4}$ and will increase nearly three-fold in going from 2700 K to 1400 K. A much better choice for the study would have been a value of $N'' \approx 10$ which would have flattened out this temperature dependence. However this is not possible using the XeCl excimer laser. An alternative approach would be to use a doubled dye laser to pump the (1,0) band or to use the KrF excimer as Raman shifted in D_2 to pump the (2,0) band. The later approach should provide approximately 25 mJ of useable energy from 267.7 to 268.9 nm thus access to strong transitions with near optimal values for N'' in the (2,0) band as well as freedom from radiation trapping effects.

Collisional effects play an important role in the description of the dependence of the fluorescence signal on the distribution of flow scalars. Pumping to predissociated states of OH does yield a reasonably well-defined dependence, however, the signal levels are too low for single-shot PLIF imaging. When this technique is applied to flows that produce a noticeable VET rate (e.g. vitiated air) the signal will be further reduced by the need to reject emission from $v' \neq 3$. Predissociated techniques can be successful for single-shot imaging and for relatively small flows when the target molecule is a major species and exhibits a large absorption cross-section (e.g. NO $D^2\Sigma$-$X^2\Pi$ as a flow tracer or O_2 $B^3\Sigma$-$X^3\Sigma$). Since OH is generally a minor species and the predissociated states exhibit a relatively small absorption cross-section, PLIF using predissociated states of OH is probably relegated to time-averaged imaging. In many cases, the total cross-section for electronic quenching of OH $A^2\Sigma(v' < 3)$ will contribute a relatively weak dependence on flow scalars, although a reasonably well-defined dependence can be elucidated. In either case,

† (private communication: Dr. P. Andresen, Max-Planck Inst, Göttingen, 1989)

quantitative measurements will need to be based on ratiometric image processing, which to a large extent can cancel-out these collisional effects[2].

CONCLUSIONS

Planar laser-induced fluorescence imaging of OH has been conducted in the exhaust of an H_2/O_2 fueled rocket engine. Tests have been made using both OH (0,0) and (3,0) excitation, the former being collisional quenching and the latter predissociation dominated. The measurements support a view that single-shot PLIF measurements of OH using predissociated excited states will not yield sufficient signal for flow visualization studies much less quantitative imaging. As expected $Q_1(3)$ (0,0) excitation was found to be subject to beam attenuation and presumably radiation trapping. For flow studies of small engines use of the weaker $R_2(3)$ (0,0) transition will provide a convenient means to reduce laser beam attenuation to acceptable levels. For the conditions expected in engine exhausts radical species have been identified as having a significant role in collisional dexcitiation; specifically OH as a VET partner via 'near-resonant' exchange and atomic hydrogen as a quenching partner. To avoid beam attenuation, to minimize the effect of radiation trapping and to reduce the dependence on temperature, a scheme based on pumping the (2,0) band has been proposed. This may be conveniently performed by using D_2 Raman shifted radiation from the injection seeded KrF excimer laser.

ACKNOWLEDGEMENTS

The authors would like to acknowledge Mr. J. Muss and Ms. J. Griggs of Gencorp Aerojet for assistance with the experimental setup and for the thermal analysis and instrumentation of the engine. Dr. Paul and Dr. Clemens are supported by the Department of Energy, Office of Basic Energy Sciences, Division of Chemical Sciences.

APPENDIX A

Collisional effects in OH $A^2\Sigma$ have been studied in some detail[12]. However, there is only limited experimental data for temperatures above 1200 K and little or no data for $v' > 1$. Thus we resort to a model of the process to extrapolate the experimental data base to the conditions of interest. This model is based on the assumption that the gross behavior of quenching and vibrational relaxation in OH $A^2\Sigma$ is described by long lived collision-complexes[13]. The rate for process W (electronic quenching or vibrational relaxation), due to collision partners p, is given by

$$W = n_0 \langle v_{OH} \rangle \sum_p \chi_p \sigma_{W,p}(T,N') \sqrt{(1+m_{OH}/m_p)} \qquad (A.1)$$

Here σ is the species and process specific thermally averaged cross-section, which is a function of temperature and rotational level. Taking a classical approach, the cross-section is given by

$$\sigma_W = \pi \int_v \int_\Theta v f_B(v,\Theta) \int_b P_W(b,v,\Theta)\, db^2\, d\Theta\, dv / \langle v \rangle \qquad (A.2)$$

Here P_W is the probability of process W occurring upon collision as a function of the collision impact parameter b, the relative velocity v, and relative molecular orientation Θ. In the model we take P_W to be a product of the probability for capture within a barrier formed by centripetal repulsion and molecular attraction, and a constant probability for the specific process, P_Q or P_V. We take the attractive forces to be given by point multipole expansions. With these assumptions equation (A.2) reduces to a 6-fold nested integral which contains a set of transcendental equations. Previous approaches to a solution have taken the collision partners to be in the orientation most favorable for dipole-dipole interactions; this reduces the problem to a single integral over a transcendental equation[14]. We find that by neglecting the quadrapole-quadrapole and higher multipole terms and by transforming to a radial integral metric the problem reduces to a three-fold integral over an explicit function and can be easily evaluated.

The present formulation does not introduce a direct dependence on rotational level and the model does not provide an absolute value for the cross-section. Thus we assume that: solutions for OH in the most attractive orientation correspond to the case of $N'' = 0$; and solutions for OH with a geometrically averaged potential correspond to the case of $N'' >> 1$. Analytical perturbation solutions in these limits suggest the functional form,

$$\sigma(T,N') \approx \sigma(T_r,0)\, y^{-p1}\, ((B_{N'} + b\, y)/(1 + b))^{p2} \qquad (A.3)$$

where $y \equiv T/T_r$ and $B_{N'}=1$ for $N'=0$ and goes to zero for large N'. The coefficients p1, p2 and b are collision partner specific and are determined from fits to the results of the full simulation, where the inputs are molecular electrical properties. Using the suggestion of Crosley[12] we take $B_{N'} = exp(-aN'(N'+1))$. Experimental data at $T_r = 300$ K are used to provide the coefficients $\sigma(T_r,0)$ and a, which are collision partner and process specific.

Simulations have been evaluated for all of the major collision partners present in the H_2/air combustion system. Comparisons to the available experimental data are favorable for all species except for electronic quenching by N_2 although VET by N_2 is well described. One possible explanation is that the necessary mixing of internal states required for quenching by N_2 introduces a strong orientation dependence. In the present model this detail has be relegated to the constant P_Q. By using N_2 quenching data for $N' \geq 3$ to provide the fit we find a significantly better match to measurements at 1200 K. Compared to the use of the 'optimum dipole' result[15], this formulation provides a significant improvement in the prediction of high temperature behavior for all of the species. Full tabulation of these results is beyond the scope of the present paper but we give as example the terms for quenching OH $A^2\Sigma$ ($v'=0$) by H_2O: $\sigma_0 = 94.1$, p1 = 0.667, a = 0.019, b = 0.21, and p2 = 0.33.

REFERENCES

1 R. K. Hanson, J. M. Seitzman and P. H. Paul, 'Planar laser-induced fluorescence imaging in combustion gases,' Appl. Phys. **B 40**, pp 441 (1990). R. K. Hanson 'Combustion diagnostics: planar imaging techniques,' in *Proc. 21st Symposium (international) on Combustion*, (The Combustion Inst., 1986), pp 1677.

2 P. H. Paul, U. E. Meier, and R. K. Hanson, 'Single-shot, multiple-camera planar laser-induced fluorescence imaging in gaseous flows,' AIAA 29th Aerospace Sciences Conf. (1991), AIAA-91-0459.

3 P. H. Paul, M. P. Lee and R. K. Hanson, 'Quantitative imaging of temperature fields in air using planar laser-induced fluorescence imaging of O_2,' Opt. Letts. **12**, pp 75, (1987).

4 J. M. Seitzman, A. Üngüt, P. H. Paul and R. K. Hanson, 'Imaging and characterization of OH structures in a turbulent nonpremixed flame,' in *Proc. 23rd Symposium (international) on Combustion*, (The Combustion Inst., 1991), pp 637.

5 P. H. Paul, 'The application of intensified array detectors to quantitative planar laser-induced fluorescence imaging,' AIAA 27th Joint Prop. Conf. (1991), AIAA 91-2315.

6 P. Andresen, A. Bath, W. Gröger, H. W. Lülf, G. Meijer and J. J. ter Meulen, 'Laser-induced fluorescence with tuneable excimer lasers as a possible method for instantaneous temperature field measurements at high pressures: check with an atmospheric flame,' Appl. Opt. **27**, pp 365, (1988).

7 R. W. Pitz, T. S. Cheng, S. R. March and J. A. Wehrmeyer, 'Effects of swirl on finite-rate chemistry in lifted jet diffusion flames,' AIAA 27th Joint Propulsion Conf. (1991), AIAA 91-2319.

8 J. M. Seitzman, *Quantitative applications of fluorescence imaging in combustion*,' Doctoral Dissertation, (Stanford Univ. 1991), HTGL report T-275.

9 J. T. Yardley, *Introduction to molecular energy transfer*, (Academic, 1980).

10 L. A. Melton and W. Klemperer, JCP **55**, pp 1468, (1971). R. G. Gordon and Y-N. Chiu 'On a first-order electronic dipole-dipole mechanism for energy transfer in molecular collisions,' JCP **55**, pp 1469, (1971).

11 R. J. Cross and R. G. Gordon, 'Long-range scattering from anisotropic potentials: dipole-dipole scattering,' JCP **45**, pp 3571 (1966).

12 D. R. Crosley, 'Rotational and translational effects in collisions of electronically excited diatomic hydrides,' JPC **93**, pp 6273 (1989).

13 R. K. Lengal and D. R. Crosley, 'Rotational dependence of vibrational relaxation in $A^2\Sigma^+$ OH,' Chem. Phys. Letts. **32**, pp 261 (1975).

14 P. W. Fairchild, G. P. Smith and D. R. Crosley 'Collisional quenching of $A^2\Sigma^+$ OH at elevated temperatures,' JCP **79**, pp 1795 (1983).

15 R. A. Copeland and D. R. Crosley, 'Temperature dependent electronic quenching of OH($A^2\Sigma^+$,v'=0) between 230 and 310 K,' JCP **84**, pp 3099 (1986). N. L. Garland and D. R. Crosley, 'On the collisional quenching of electronically excited OH, NH and CH in flames,' in *Proc. 21st Symposium (international) on Combustion*, (The Combustion Inst., 1986), pp 1693.

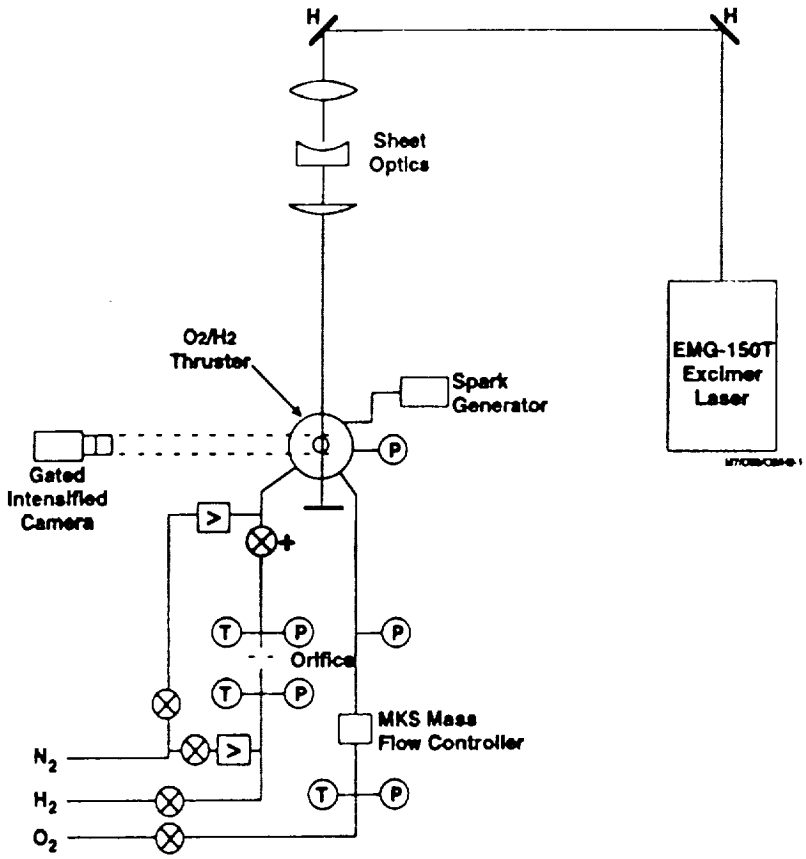

Figure 1. Schematic of the experimental setup.

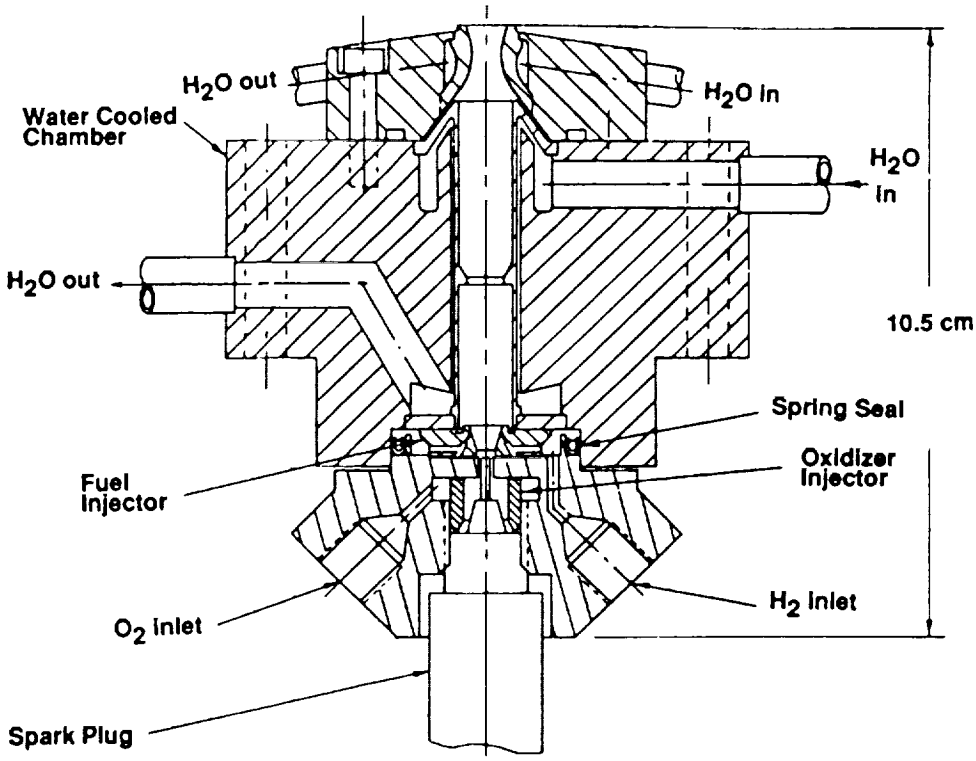

Figure 2. Schematic of the subscale 5 lbf thrust rocket engine.

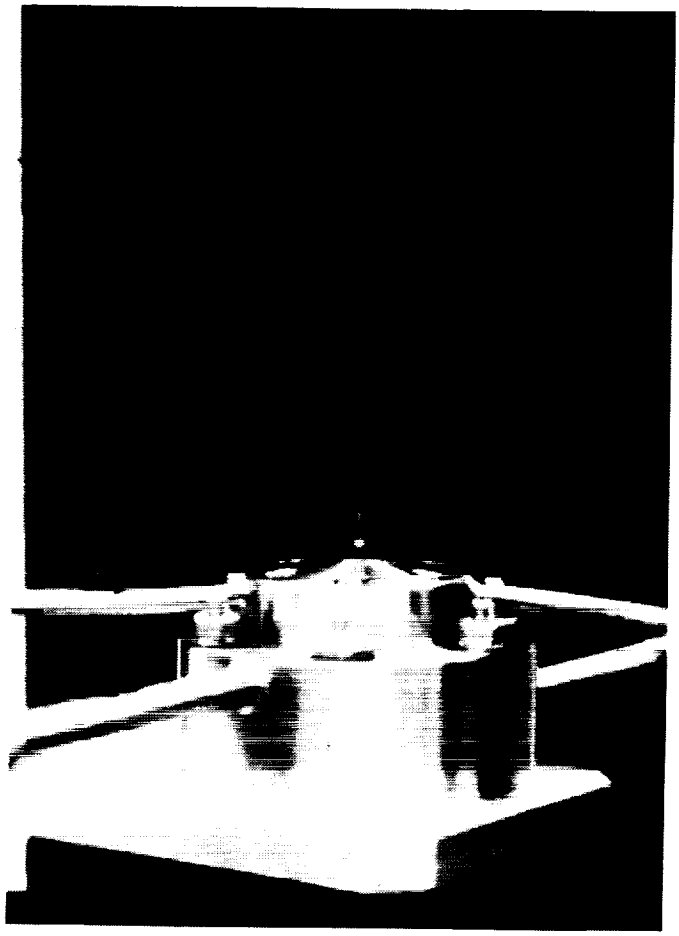

Figure 3. Conventional time-exposure photograph of the natural emission from the engine exhaust plume.

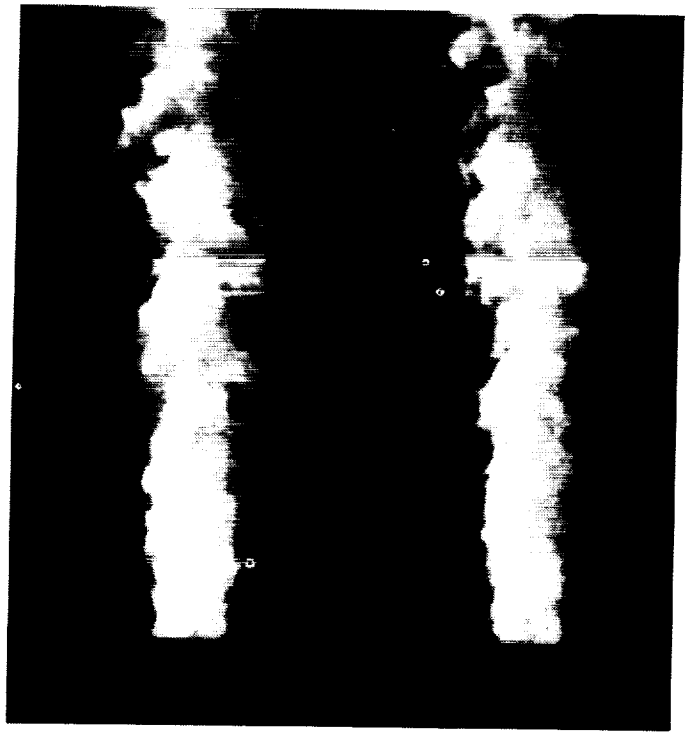

Figure 4. Two single-shot PLIF images of OH in the engine exhaust plume, obtained by pumping the (0,0) band.

Figure 5. Two single-shot PLIF images of OH in the engine exhaust plume, obtained by pumping the (3,0) band.

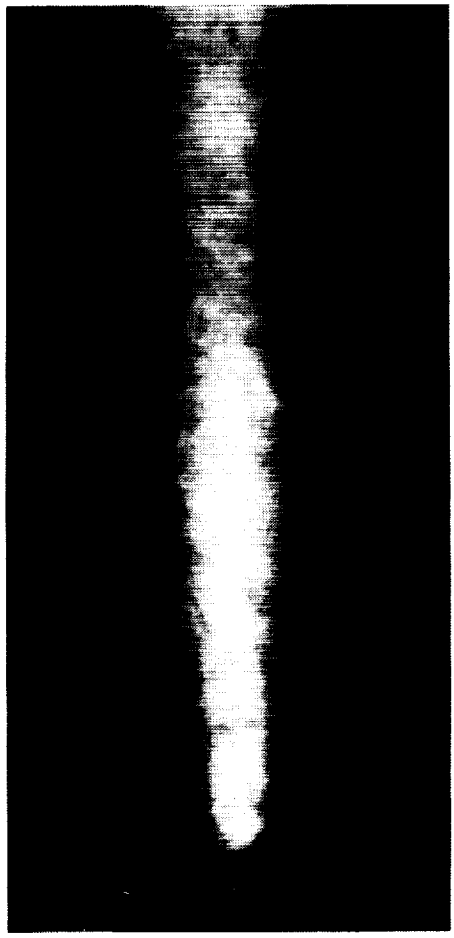

Figure 6. Fifteen frame average image of OH in the engine exhaust plume, obtained by pumping the (3,0) band.

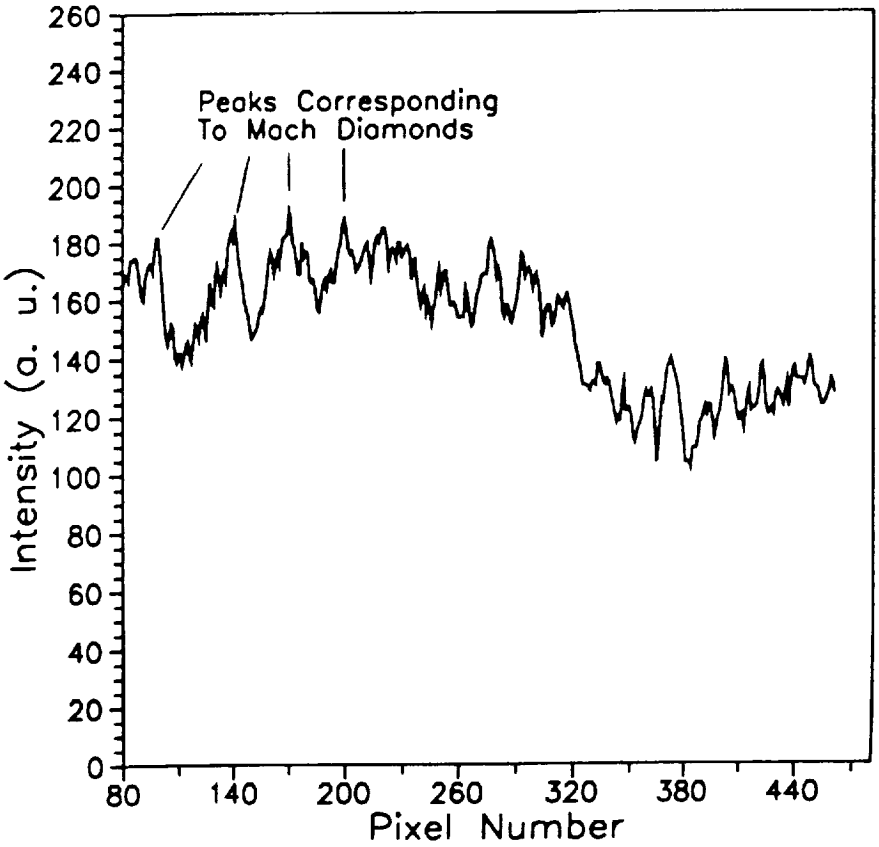

Figure 7. Pixel intensity variation taken from figure 6 and along the axis of the engine exhaust plume. The positions of the shock diamonds have been indicated.